Simulation of Immiscible WAG Injection in a Stratified Reservoir – Performance Characterization Using a New Dimensionless Number

Jan Inge Nygård[1] and Pål Østebø Andersen[1,2,3]

[1]Department of Energy Resources, University of Stavanger, 4036 Stavanger, Norway.
[2]Department of Energy and Petroleum Engineering, University of Stavanger, 4036 Stavanger, Norway.
[3]The National IOR Centre of Norway, 4036 Stavanger, Norway.
E-mails: nygaard.janinge@gmail.com, pal.andersen@uis.no

Abstract. Water-Alternating-Gas (WAG) is a well-established EOR process where gas and water are injected in alternating fashion. Good volumetric sweep is achieved as water and gas target both the oil residing in low and high portions of the reservoir, respectively. Other important features in three phase hysteretic flow include phase trapping which is believed to be more strongly associated with the gas phase. With these aspects in mind a vast simulation study has been performed investigating immiscible WAG injection focusing on mechanisms such as mobility, gravity, injected volume fractions, reservoir heterogeneity, gas entrapment and relative permeability hysteresis.

The aim of our work is to investigate the interplay between these mechanisms for a model system with sufficient complexity to be of relevance and then scale recovery performance using a new dimensionless number that incorporates the relevant model input parameters. A horizontally layered reservoir is considered where oil is displaced by water and gas alternately injected towards a producer. The model is a modified black-oil type, where hysteresis in the gas phase is modeled using Land's model for trapping and Carlsens model for relative permeability hysteresis. It is seen that gravity segregation in uniform models and increased heterogeneity in no-gravity models both lead to lower oil recovery. However, in heterogeneous models, gravity can divert flow from high permeable layers into low permeable layers and improve recovery. Hysteresis lowers gas mobility and hence improves gas-oil mobility ratio and reduces gravity segregation. The first effect is always positive, but the second is mainly positive in more uniform reservoirs where gravity segregation has a negative effect on recovery. In heterogeneous reservoirs, reducing gravity segregation can lead to that the oil in low permeable layers remains unswept.

The newly derived characteristic dimensionless number is effectively a WAG mobility ratio, termed M^* expressing how well the injected fluid mixture is able to displace oil whether it is due to fluid mobilities, heterogeneity or other effects. At a value of M^* near 1 optimal recovery is achieved, while logarithmic increase of M^* reduces recovery.

Keywords. Water-alternating-gas (WAG); Gravity segregation; Hysteresis; Heterogeneity; Dimensionless numbers and scaling

1. Introduction

Water-Alternating-Gas (WAG) is an Enhanced Oil Recovery (EOR) process initially intended for conformance control during gas flooding (van Lingen et al., 1996). However, it has also been demonstrated superior to water flooding (Christensen et al., 2001). Alternately injecting water and gas capitalizes on the improved microscopic displacement efficiency by gas and the improved mobility control and volumetric sweep efficiency by water (Chen and Reynolds, 2016; Talabi et al., 2019). One way this occurs is by formation of a three-phase mixing zone that sweeps a larger portion of the reservoir compared to continuous gas injection (Namani et al., 2017). This also increases the potential for gas entrapment (Righi et al., 2004) and consequent reductions in gas relative permeability (Kumar et al., 2017), thus making the gas less mobile and less prone to bypassing of the oil phase by viscous fingering. The potential for WAG to improve oil production has been found most evident as reservoir heterogeneity increases Hoare et al. (2018). WAG is often used in carbonates that are highly heterogeneous in nature (Ahmed Elfeel et al., 2013; Pal et al., 2018). Hoare et al. (2018) applied fine grid resolution to capture heterogeneities at pore, core and larger scale (by layering of different formations) to model WAG performance on the Hutton

sandstone field in the North Sea. This field is highly heterogeneous in both horizontal and vertical direction. They predicted that immiscible WAG injection would give 10 and 5 % incremental oil recovery when hysteretic features were and were not present, respectively. By comparison, they found that WAG was not successful in a homogeneous model. Kumar et al. (2017) history matched the response from continuous-gas-injection field pilots. The option of using WAG was investigated where they found that, even without incorporation of gas entrapment and relative permeability hysteresis effects, WAG would boost recovery significantly, use less gas and reduce water-cut.

Immiscible WAG is used when reservoir heterogeneities would worsen gravity segregation if single-phase injection was used (Baojun et al., 1997; Christensen et al., 2001). Water and gas are less sensitive to the surrounding heterogeneous rock in the three phase mixing zone, where they move at comparable speeds. That also helps to negate the effect of unfavorable mobility ratio. Outside of this zone, and especially with layering of different properties, their differences become more pronounced. If the mixing zone is not maintained, gravity segregation can be enhanced by heterogeneity and cause negative influence on oil recovery (Genrich et al., 1986; Surguchev et al., 1992). Namani et al. (2017) performed laboratory investigations on water-above-gas WAG injection. The segregation distance from the injector was shown to be extended compared to regular WAG injection. This was attributed mainly to trapping of gas, but also improved overall mobility and reduced gravity segregation.

Measures should be taken to optimize injectivity and the size of the mixing zone in both low and high permeable layers. Surguchev et al. (1992) states that the governing parameters determining this behaviour are the WAG ratio and injection rate. The optimal WAG ratio was referred to by van Lingen et al. (1996) as the ratio at which the injected phases (gas and water) move at equal velocity and in the same direction in the reservoir. In a sector model history-matched to data from a (mostly) immiscible WAG injection pilot, Pal et al. (2018) found that a WAG ratio of 1:1 was favorable over non-equal WAG ratios due to achieving a more stable oil production rate that was less prone to fluctuations. By shortening both gas and water slug cycle durations from 6 months to 1 month, the oscillations in oil rate became negligible and the ultimate oil recovery higher. This might be explained by the mobility reduction resulting from WAG, which appears to occur even in absence of hysteretic features as seen in numerical simulations (Kumar et al., 2017; Pal et al., 2018). The hysteretic effects may become enhanced from a more frequent switching of injectant fluid. However, WAG injection does not always exhibit strong cyclic hysteresis, and in some cases it is not significant (Alzayer and Sohrabi, 2018).

As the degree of heterogeneity increases, ie. with layers within the formation, multiphase flow becomes more sensitive to accurate measurement and modelling of three phase relative permeabilities (Sedaghat and Azizmohammadi, 2018) and related hysteretic effects (Khorsandi et al., 2017; Alzayer and Sohrabi, 2018). Shahverdi and Sohrabi (2014) found experimentally that the non-wetting phase underwent much stronger hysteresis than the wetting phase. The gas phase is thus often expected to show large hysteretic effects (Hoseini et al., 2011). Shahverdi and Sohrabi (2016) highlighted that the cyclic dependency of relative permeability should be captured. Kamali et al. (2017) also mentioned that injected water may prevent contact between the injected gas and in-situ oil, and thus reduce the overall microscopic displacement efficiency.

This work presents a WAG simulation study considering some of the key mechanisms pointed out in the literature. Oil is recovered from a layered reservoir and the WAG operation is considered under different fluid-rock and well parameter configurations. We limit our investigations to consider immiscible and incompressible fluids, and focus on the role and interplays of mobility, gravity, hysteresis, phase-dependent microscopic sweep and reservoir heterogeneity. Compressibility and miscibility effects are hence ignored in this study. Under these conditions our aim is to address key questions such as:

- Which mechanisms determine whether WAG is a better alternative than single phase injection?
- What determines the extent of gravity segregation and how is that influenced by reservoir heterogeneity and hysteresis?
- Can WAG injection performance be predicted?

These questions will be addressed by performing simulations and scaling the results. The paper is structured as follows: (1) The model assumptions, geometry and governing equations are presented. (2) A dimensionless characterizing number is presented to be applied for scaling the simulation results. (3) Input correlations and base case parameters are listed. (4) Sensitivity analyses are carried out to demonstrate the general behaviour of the WAG process, mechanisms and flow regimes. The ability of the dimensionless number to scale recovery is demonstrated by systematically determining parameters related to each mechanism. (5) The paper is finalized by discussion and conclusions.

2. Model description

2.1. **Geometry.** We consider a stratified reservoir as illustrated in Figure 1. The layers (strata) are aligned with the horizontal x-axis which points from the injector well to the producer well. The layers are internally homogeneous (uniform height, porosity and permeability), but may individually have different properties. The z-axis points downwards along the direction of gravity, normal to the injector-producer path. The wells are considered to operate on the entire vertical interval.

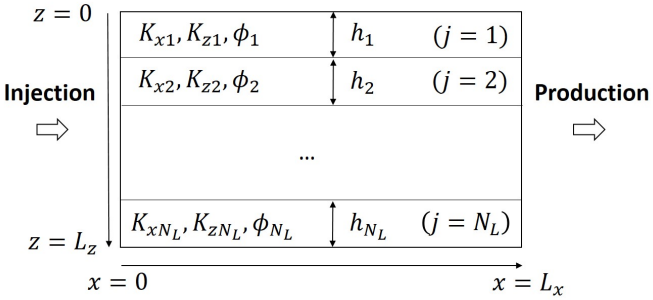

Figure 1. System geometry.

2.2. **Mathematical description.** We assume flow of three incompressible, immiscible fluids oil (o), water (w) and gas (g) in the incompressible porous subsurface. Relevant conservation laws together with Darcy's law (Chen et al., 2006) are given by:

$$\phi \partial_t s_i = -\nabla \cdot \mathbf{u}_i, \qquad \mathbf{u}_i = -\frac{\mathbf{K} k_{ri}}{\mu_i}\Big(\nabla p_i - \rho_i g \nabla \mathbf{z}\Big), \qquad (i = o, w, g) \tag{1}$$

with definitions ϕ porosity, s_i saturation, u_i Darcy flux, $\mathbf{K}$ absolute permeability tensor, k_{ri} relative permeability, μ_i viscosity, p_i pressure, ρ_i density, $g = 9.81$ m/s^2 acceleration of gravity and z depth. Index i denotes phase. The six variables s_i, p_i are constrained by volume conservation and capillary pressure:

$$s_o + s_w + s_g = 1, \quad p_o - p_w = P_{cow}(s_w) \quad p_g - p_o = P_{cgo}(s_g) \tag{2}$$

For the conditions considered in this work, capillary pressure effects are assumed negligible. We thus take phase pressures locally equal $p_o = p_w = p_g$ being referred to as p in the following. Adding the conservation laws in (1) gives:

$$\nabla \cdot \mathbf{u}_T \quad = \quad 0, \tag{3}$$

where the total Darcy flux vector $\mathbf{u}_T$ is defined by:

$$\mathbf{u}_T \quad = \quad \mathbf{u}_o + \mathbf{u}_w + \mathbf{u}_g = -\mathbf{K}\lambda_T \nabla p + \mathbf{K} g(\lambda_o \rho_o + \lambda_w \rho_w + \lambda_g \rho_g)\nabla \mathbf{z}, \tag{4}$$

$$\lambda_i \quad = \quad \frac{k_{ri}}{\mu_i}, \qquad \lambda_T = \lambda_o + \lambda_w + \lambda_g, \tag{5}$$

and λ_i, λ_T denote phase and total mobilities, respectively. Solving (4) for the pressure gradient ∇p and inserting the result into the conservation law in (1) gives:

$$\partial_t(\phi s_i) = \nabla \cdot (f_i \mathbf{u}_T) + \nabla \cdot \Big[\mathbf{K}\lambda_i g\Big(f_o(\rho_o - \rho_i) + f_w(\rho_w - \rho_i) + f_g(\rho_g - \rho_i)\Big)\nabla \mathbf{z}\Big], \tag{6}$$

$$f_i = \frac{\lambda_i}{\lambda_T}, \qquad (i = o, w, g). \tag{7}$$

f_i denotes the fractional flow function of phase i. For simplicity we consider flow in a two-dimensional setting and thus assume uniform properties along the y-direction. The equations we consider are then:

$$\begin{aligned} \partial_x u_{Tx} + \partial_z u_{Tz} &= 0 \\ u_{Tx} &= -K_x \lambda_T \partial_x p, \\ u_{Tz} &= -K_z \lambda_T \partial_z p + K_z g(\lambda_o \rho_o + \lambda_w \rho_w + \lambda_g \rho_g), \end{aligned} \tag{8}$$

and:

$$\begin{aligned} \partial_t(\phi s_o) &= \partial_x(f_o u_{Tx}) + \partial_z(f_o u_{Tz}) + \partial_z\Big(K_z g \lambda_w f_o \Delta\rho_{wo}\Big) - \partial_z\Big(K_z g \lambda_g f_o \Delta\rho_{og}\Big) \\ \partial_t(\phi s_w) &= \partial_x(f_w u_{Tx}) + \partial_z(f_w u_{Tz}) - \partial_z\Big(K_z g \lambda_o f_w \Delta\rho_{wo}\Big) - \partial_z\Big(K_z g \lambda_g f_w \Delta\rho_{wg}\Big) \end{aligned} \tag{9}$$

where:

$$\Delta\rho_{wo} \;=\; \rho_w - \rho_o, \quad \Delta\rho_{wg} = \rho_w - \rho_g, \quad \Delta\rho_{og} = \rho_g - \rho_o. \tag{10}$$

The flow field $u_T = (u_{Tx}, u_{Tz})$ follows from solving the pressure equation (8). The flow field is applied in (9) to update the saturation distributions s_o, s_w with time. s_g follows from the saturation constraint. The equations in (8) and (9) thus constitute the governing equations considered in this work.

2.3. **Relative permeability and hysteresis.** Relative permeabilities are defined with Corey formulation (Brooks and Corey, 1964) as follows:

$$\begin{aligned} k_{rw} &= k_{rw}^{max}\Big(\frac{s_w - s_{wc}}{s_{w,max} - s_{wc}}\Big)^{n_w}, \quad (s_{wc} < s_w < s_{w,max}); \\ k_{rw} &= 0, \quad (0 < s_w < s_{wc}), \\ k_{row} &= k_{row}^{max}\Big(\frac{s_{ow} - s_{orw}}{s_{ow,max} - s_{orw}}\Big)^{n_{ow}}, \quad (s_{orw} < s_{ow} < s_{ow,max}), \\ k_{row} &= 0, \quad (0 < s_{ow} < s_{orw}), \\ k_{rg} &= k_{rg}^{max}\Big(\frac{s_g - s_{gr}}{s_{g,max} - s_{gr}}\Big)^{n_g}, \quad (s_{gr} < s_g < s_{g,max}), \\ k_{rg} &= 0, \quad (0 < s_g < s_{gr}), \\ k_{rog} &= k_{rog}^{max}\Big(\frac{s_{og} - s_{org}}{s_{og,max} - s_{org}}\Big)^{n_{og}}, \quad (s_{org} < s_{og} < s_{og,max}), \\ k_{rog} &= 0, \quad (0 < s_{og} < s_{org}), \\ s_{w,max} &= 1 - s_{orw}, \quad s_{ow,max} = 1 - s_{wc}, \\ s_{g,max} &= 1 - s_{wc} - s_{org}, \quad s_{og,max} = 1 - s_{wc} - s_{gr}. \end{aligned} \tag{11}$$

Water-oil relative permeabilities k_{rw}, k_{row} are functions of s_w only, where $s_{ow} = 1 - s_w$. Gas-oil relative permeabilities k_{rg}, k_{rog} are functions of s_g only and measured in presence of critical water saturation $s_w = s_{wc}$, where $s_{og} = 1 - s_g - s_{wc}$. During simulation a standard combination of k_{row} and k_{rog} are used as a measure of the relative permeability of oil:

$$k_{ro}(s_w, s_g) = \frac{s_g k_{rog} + (s_w - s_{wc})k_{row}}{s_g + s_w - s_{wc}}. \tag{12}$$

Hysteresis is implemented using the WAGHYSTR hysteresis model in ECLIPSE, which combines elements from Land (1968) and Carlson (1981). Land (1968) used pore-size distribution

and capillary pressure data from sands to develop a characteristic rock-parameter C (assumed constant):

$$C = \frac{1 - s_{wc}}{(s_{gr})_{max}} - 1, \qquad s_{g,trap} = s_{gr} + \frac{s_{g,m} - s_{gr}}{1 + C(s_{g,m} - s_{gr})} \tag{13}$$

to predict hysteretic features when the non-wetting phase saturation changed direction from increasing to decreasing. The highest gas saturation attained before the turn, $s_{g,m}$, is used to calculate the trapped gas saturation $s_{g,trap}$, at which gas mobility is then zero (see illustration left in Figure 2). A lowered relative permeability for gas due to entrapment is then calculated involving an analytical version of the Carlson (1981) model. Specifically, the Carlson mapping algorithm is used to overcome unphysically steep relative permeability curves (and related convergence issues) when input values approach limiting boundaries. If gas saturation should increase again (as is expected during WAG), a parameter α defines the extent at which the mobility is able to increase with increasing gas saturation, compared to the saturation path taken for decreasing gas saturation, see right in Figure 2. Geffen et al. (1951) noted significant gas entrapment when a previously gas flooded medium was flooded with water afterwards. They estimated that maximum residual gas saturation (due to hysteresis) would be in the order of 15 to 50 %. Fatemi et al. (2012) performed a number of laboratory investigations into gas-water systems and found that gas entrapment ranged from around 20 to 30 %.

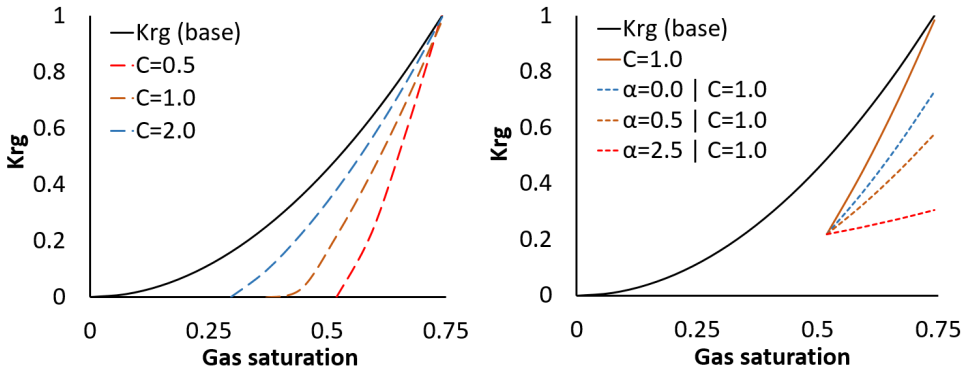

FIGURE 2. The role of hysteresis parameters C (left) and α (right) on gas relative permeability.

2.4. **Initial and boundary conditions.** At initial state, water and gas are at residual saturation, while oil is at maximum saturation.

$$s_o(t = 0) = 1 - s_{wr} - s_{gr}, \qquad s_w(t = 0) = s_{wr}, \qquad s_g(t = 0) = s_{gr}. \tag{14}$$

All sides of the model are closed and all mass transfer with the surroundings happens through the injector and producer wells.

2.5. **Numerical solution of equations.** The system equations (8) to (14) were solved fully implicit using the commercial software ECLIPSE 100 (GeoQuest, 2014). The relative permeabilities and the mentioned hysteresis model were implemented using the key words SWOF, SGOF and WAGHYSTR. The grid was discretized using $N_x = 100$ cells in x-direction and $N_z = 81$ cells in z-direction (at least 9 cells in the vertical direction per layer in our examples), while the max time step was limited by the default value of 365 d (but in practice limited by max changes in saturation and pressure). The impact of refining grid or the maximum time step are shown in Appendix B. Some grid sensitivity was observed for the most challenging cases (with heterogeneity, hysteresis, gravity and WAG acting at once) while for less challenging cases, there was negligible impact. Moreno and Flew (2011) indicated that low vertical grid resolution could give too optimistic results. Talabi et al. (2019) found that when the ratio of the resolution of an upscaled grid to the base resolution (0.015 ft) of a coreflood grid exceeded 2500:1, the degree of trapped gas (and recovered oil) declined rapidly from a stable level.

3. Methodology of characterization

Our aim is to develop a dimensionless number that can correlate and roughly predict recovery performance during WAG injection. In the following we evaluate various mechanisms and propose how they can be incorporated into such a number. We propose a universal mobility ratio that accounts for all effects leading to imperfect displacement of oil for a given injected volume.

3.1. **Mobility.** As documented in the literature (Craig Jr et al., 1955; Habermann, 1960) for twophase flow; the recovery performance is strongly associated with the displacing-over-displaced phase mobility ratio M which can be defined for water-oil $M_{w/o}$ and gas-oil $M_{g/o}$:

$$M_{w/o}(s_w) = \frac{\lambda_w}{\lambda_{ow}} = \frac{\mu_o}{\mu_w}\frac{k_{rw}}{k_{row}}, \quad M_{g/o}(s_g) = \frac{\lambda_g}{\lambda_{og}} = \frac{\mu_o}{\mu_g}\frac{k_{rg}}{k_{rog}}, \tag{15}$$

evaluated at a characteristic value. However, as demonstrated in Appendix A, even for a simple Buckley-Leverett scenario (Buckley and Leverett, 1942) two parameters are required to give a unique prediction. We evaluate the relative permeabilities by their average over their full saturation interval $s_i = 0, .., s_{i,max}$ (where $s_{i,max}$ is the saturation where the highest relative permeability k_{ri}^{max} is obtained and $i = w, ow, g, og$) and obtain:

$$\begin{aligned} k_{ri}^* &= \frac{1}{s_{i,max} - 0}\Big[\int_{s_i=0}^{s_{ir}} 0 ds_i + \int_{s_i=s_{ir}}^{s_{i,max}} k_{ri}^{max}\Big(\frac{s_i - s_{ir}}{s_{i,max} - s_{ir}}\Big)^{n_i} ds_i\Big] \\ &= \Big(1 - \frac{s_{ir}}{s_{i,max}}\Big)\frac{k_{ri}^{max}}{(n_i + 1)}. \end{aligned} \tag{16}$$

Characteristic twophase mobility ratios can then be defined as:

$$\begin{aligned} M_{w/o}^* &= \frac{\lambda_w^*}{\lambda_{ow}^*} = \frac{\mu_o}{\mu_w}\frac{k_{rw}^{max}}{k_{row}^{max}}\frac{(n_{ow}+1)}{(n_w+1)}\frac{\Big(1 - \frac{s_{wr}}{s_{w,max}}\Big)}{\Big(1 - \frac{s_{orw}}{s_{ow,max}}\Big)}, \\ M_{g/o}^* &= \frac{\lambda_g^*}{\lambda_{og}^*} = \frac{\mu_o}{\mu_g}\frac{k_{rg}^{max}}{k_{rog}^{max}}\frac{(n_{og}+1)}{(n_g+1)}\frac{\Big(1 - \frac{s_{gr}}{s_{g,max}}\Big)}{\Big(1 - \frac{s_{org}}{s_{og,max}}\Big)}. \end{aligned} \tag{17}$$

3.2. **Heterogeneity.** Considering that the model may consist of heterogeneous layers it is natural to assume that flow will be diverted to the most permeable layers leading to quicker breakthrough of the displacing phase. We hence define a heterogeneity multiplier F_H to indicate how heterogeneity increases the effective mobility ratio:

$$F_H = \frac{\overline{K}_x^{arit}}{\overline{K}_x^{harm}} \geq 1, \tag{18}$$

where we have defined arithmetic and harmonic averages of horizontal permeabilities as:

$$\overline{K}_x^{arit} = \frac{1}{L_z}\sum_{j=1}^{N_L} h_j K_{x,j}, \qquad \overline{K}_x^{harm} = L_z\Big(\sum_{j=1}^{N_L}\frac{h_j}{K_{x,j}}\Big)^{-1}, \qquad L_z = \sum_{j=1}^{N_L} h_j. \tag{19}$$

N_L is the number of layers. Note that due to the properties of the means (Xia et al., 1999) we obtain $F_H = 1$ if and only if all horizontal permeabilities are the same, while otherwise heterogeneity implies $F_H > 1$.

3.3. **Gravity.** The extent of gravity segregation during injection depends on (a) the time required for the phases to reach their vertical equilibrium distribution as determined by their relative densities (and capillary pressure if significant) compared to (b) the time the fluids have available in the reservoir to do so. The former is denoted segregation time and can be written as follows

for water-oil and gas-oil:

$$t_{seg}^{w/o} = \frac{H\phi}{K_z^{harm}\Delta\rho_{wo}g}\Big(\frac{1}{\lambda_w^*} + \frac{1}{\lambda_{ow}^*}\Big),$$
$$t_{seg}^{g/o} = \frac{H\phi}{K_z^{harm}\Delta\rho_{go}g}\Big(\frac{1}{\lambda_g^*} + \frac{1}{\lambda_{og}^*}\Big). \tag{20}$$

These expressions are similar to the time scale for gravity drainage proposed by Hagoort (1980). The latter time scale is taken as the residence time of the injected fluid, t_{res}, corresponding to the time of injecting one pore volume.

$$t_{res}^{w} = \frac{L_x L_y \sum_{j=1}^{N_L}\phi_j h_j}{Q_w}, \qquad t_{res}^{g} = \frac{L_x L_y \sum_{j=1}^{N_L}\phi_j h_j}{Q_g}, \tag{21}$$

where L_y is the width of the reservoir. Taking the ratio of residence and segregation time scales we obtain water-oil and gas-oil gravity numbers N_G:

$$N_G^{w/o} = \frac{t_{res}^{w/o}}{t_{seg}^{w/o}}, \qquad N_G^{g/o} = \frac{t_{res}^{g/o}}{t_{seg}^{g/o}}. \tag{22}$$

If $N_G >> 1$ there will be segregation between the indicated phases. If the injected phase does not segregate with oil, it should displace oil according to its mobility ratio. In a uniform reservoir ($F_H = 1$) gravity should lead to segregation and less effective displacement, i.e. $F_G \geq 1$. It is reasonable to assume the following gravity factor:

$$F_G^{w/o} = 1 + a_1(N_G^{w/o})^{a_2}, \qquad F_G^{g/o} = 1 + a_1(N_G^{g/o})^{a_2}, \tag{23}$$

where $a_1, a_2 > 0$ are fitting parameters determining for which gravity numbers segregation is significant and how it impacts oil recovery. In heterogeneous models, gravity effects were found to be coupled with heterogeneity and the following extension of (23) was applied:

$$F_G^{w/o} = \frac{1 + a_1(N_G^{w/o})^{a_2}}{1 + a_1(F_H - 1)(N_G^{w/o})^{a_2}}, \qquad F_G^{g/o} = \frac{1 + a_1(N_G^{g/o})^{a_2}}{1 + a_1(F_H - 1)(N_G^{g/o})^{a_2}}. \tag{24}$$

We underline that a_1, a_2 were kept fixed for all cases (matched to 3 and 0.5, respectively). Note that at $F_H = 1$ we obtain (23) and that for large F_H, F_G can become less than 1, although not lower than $1/F_H$.

3.4. **Hysteresis.** Hysteresis in our model works by altering the relative permeability of gas k_{rg}. This is implemented in the scaling by reducing the mobile saturation interval or by lowering the end point relative permeability. First, for a given C, a critical gas saturation s_{gr}^{hyst} after *maximum hysteresis* is calculated according to (13) evaluated at $s_g = s_{g,max}$.

$$s_{gr}^{hyst} = s_{gr} + \frac{s_{g,max} - s_{gr}}{1 + C(s_{g,max} - s_{gr})}. \tag{25}$$

We note that if we inject only gas ($r_w = 0$) the saturation changes are monotonous and there can be no hysteresis, while for $r_w \approx 1$ any injected gas will be subject to severe saturation changes. The relevant critical gas saturation is then:

$$s_{gr}^{wag} = s_{gr}(1 - r_w) + r_w s_{gr}^{hyst}. \tag{26}$$

s_{gr}^{wag} replaces s_{gr} in $M_{g/o}^*$, see (17). This reduces the average mobility of the gas since more of the saturation interval obtains zero mobility. Further, the parameter α is used to lower the end point gas relative permeability such that when $\alpha = 0$ there is no change, and when $\alpha \to \infty$ it approaches zero. The following correlation with α was applied:

$$k_{rg,M}^{max,hyst} = \frac{k_{rg}^{max}}{1 + b_1 F_H^{b_2}\alpha}, \quad k_{rg,N_G}^{max,hyst} = \frac{k_{rg}^{max}}{1 + b_3 F_H^{b_4}\alpha}. \tag{27}$$

These formulations capture that hysteresis results in a lower gas mobility (but have different impact for flow in horizontal and vertical direction depending on the tuning parameters b_1, b_2, b_3, b_4). This

gives a more favorable (lower) gas-to-oil mobility ratio $M^*_{g/o}$ and a lower gas-to-oil gravity number $N_G^{g/o}$. Also here, the volume fraction is incorporated:

$$k^{wag}_{rg,M} = \Big(\frac{1-r_w}{k^{max}_{rg}} + \frac{r_w}{k^{max,hyst}_{rg,M}}\Big)^{-1}, \quad k^{wag}_{rg,N_G} = \Big(\frac{1-r_w}{k^{max}_{rg}} + \frac{r_w}{k^{max,hyst}_{rg,N}}\Big)^{-1}. \tag{28}$$

The expressions (26) and (28) are then used to update mobility terms,

$$\lambda^*_{g,M} = \frac{1}{\mu_g}\Big(1 - \frac{s^{wag}_{gr}}{s_{g,max}}\Big)\frac{k^{wag}_{rg,M}}{n_g+1}, \quad \lambda^*_{g,N_G} = \frac{1}{\mu_g}\Big(1 - \frac{s^{wag}_{gr}}{s_{g,max}}\Big)\frac{k^{wag}_{rg,N_G}}{n_g+1}, \tag{29}$$

where $\lambda^*_{g,M}$ and λ^*_{g,N_G} replaces λ^*_g in $M^*_{g/o}$ for (17) and $t^{g/o}_{seg}$ for (20), respectively.

3.5. **WAG mobility ratio.** We then introduce a WAG mobility ratio, which expresses how favorable the injected fluid mixture is relative to oil.

$$M^* = \Big(\frac{r_w}{M^*_{w/o}F_H F_G^{w/o}} + \frac{1-r_w}{M^*_{g/o}F_H F_G^{g/o}}\Big)^{-1}. \tag{30}$$

r_w denotes the volume fraction of water in a WAG cycle (the remaining fraction $1-r_w$ is gas). This WAG mobility ratio is a harmonically weighted average of the individual twophase mobility ratios. The following properties are apparent:

- If one phase is infinitely mobile or infinitely segregating compared to oil ($M^*_{i/o}F_G^{i/o} \to \infty$), then it will not displace oil and the displacement behavior is completely determined by heterogeneity and the mobility ratio and gravity number between the other displacing phase and oil. If very different mobility ratios appear, it is natural that the favorable one should play a greater role in displacing oil.
- In case the injected fraction approaches single phase the WAG mobility ratio approaches the corresponding twophase mobility ratio between that injected phase and oil.
- The injected phase with most impact has high volume fraction, low mobility ratio and is assisted by gravity.
- Hysteresis affects M^* through $M^*_{g/o}$ and $F_G^{g/o}$.

For reference we also present results against the simplified mobility ratio M_{WAG} which does not account for gravity, heterogeneity or hysteresis:

$$M_{WAG} = \Big(\frac{r_w}{M^*_{w/o}} + \frac{1-r_w}{M^*_{g/o}}\Big)^{-1}, \tag{31}$$

which corresponds to (30) for $F_H = F_G = 1$ and no impact hysteresis.

4. Results and discussion

In this section we investigate the model response to viscosity, layer permeabilities, fluid densities, and hysteresis parameters which affect mobility, gravity, heterogeneity and gas entrapment. The results are compared in terms of oil recovery factor RF after 1.5 pore volumes (PVs) have been injected under gas, water or WAG injection (as represented by the volume fraction of water in a WAG cycle, r_w). These data are first presented against the number M_{wag} and then scaled to gather the data using the proposed mobility ratio M^*. The functional relations in M^* are uniquely determined by systematically incorporating increasing degree of complexity.

4.1. **Input data.** The parameters used to set up the base case are shown in Tables 1 and 2. These inputs are used in the following sections, where case variations are identified by specification of the differing parameters. Five WAG volume fractions were considered: $r_w = 0, 0.33, 0.5, 0.67, 1$, the first and last corresponding to single phase gas and water injection, respectively. Four models with differing permeability combinations will be presented resulting in different F_H, see Table 3. Each had $N_L = 9$ layers (internally uniform), except Model 1 which was uniform and used for base case simulations.

Equal density differences were assumed, denoted by $\Delta\rho = \Delta\rho_{wo} = \Delta\rho_{og}$. Also, in the base case gravity and hysteresis effects were set negligible using a low density difference $\Delta\rho = 1$ kg/m^3 and hysteresis parameters $C = \infty, \alpha = 0$, respectively (a zero density difference would be preferable, but reoccurring stability problems prevented this choice). Later cases *with* hysteresis applied parameter values $C = 1$ and $\alpha = 2.5$. For comparison, Sedaralit et al. (2016) used $C = 2$ and $\alpha = 0.05$, Kamali et al. (2017) used α between 1 and 4, to match lab experiments and Talabi et al. (2019) matched WAG coreflood experiments using $C = 2.73$ and $\alpha = 2.4$. Note also that the viscosity-relative permeability end point combinations correspond to the same maximum mobility. Together with same Corey exponents this yields symmetrical injection conditions in the base case. The relative permeability functions are displayed in Figure 3.

By scaling the recovery performance as different effects were included, the tuning parameters shown in Table 4 were obtained.

TABLE 1. Rock / grid properties and operational parameters of base case.

N_x, -	100	L_x, m	1000	ϕ_j,-	0.30	Q_w, m^3/d	1014.6	T^{w-hc}, d	45
N_y, -	1	L_y, m	100	h_j, m	3	Q_g, m^3/d	1014.6	T^{g-hc}, d	45
N_z, -	81	L_z, m	81	N_L,-	9	r_w,-	0.5	T^{tot}, PVs	1.5

TABLE 2. Reservoir fluid and flow properties of base case.

$k_{row}^{max} = k_{row}(s_{wi})$, -	0.25	n_{ow}, -	2	μ_o, cP	5	C, -	∞
$k_{rog}^{max} = k_{rog}(s_{gi})$, -	0.25	n_{og}, -	2	μ_w, cP	1	α, -	0
$k_{rw}^{max} = k_{rw}(1 - s_{orw})$, -	0.05	n_w, -	2	μ_g, cP	0.10		
$k_{rg}^{max} = k_{rg}(1 - s_{org})$, -	0.005	n_g, -	2	λ_{ow}^{max}, cP^{-1}	0.05		
s_{oi}, -	0.842	s_{orw}, -	0.20	λ_{og}^{max}, cP^{-1}	0.05		
$s_{wi} = s_{wr}$, -	0.158	s_{org}, -	0.10	λ_{w}^{max}, cP^{-1}	0.05		
$s_{gi} = s_{gr}$, -	0.00	$\Delta\rho$, kg/m^3	1 (low)	λ_{g}^{max}, cP^{-1}	0.05		

TABLE 3. Specification of model heterogeneities. Patterns are indicated from top ($j = 1$) layer.

Model	$K_{x,j}$ [mD]	$K_{z,j}$ [mD]	F_H
1 (base)	[300] x9	[300] x9	1.0
2	[300, 100, 900] x3	[300, 100, 900] x3	2.1
3	[500, 50] x4, [500]	[500, 50] x4, [500]	3.0
4	[1000, 20] x4, [1000]	[1000, 20] x4, [1000]	12.9

TABLE 4. Parameters determined from scaling simulation results.

a_1, -	3	b_1, -	1	b_3, -	10
a_2, -	0.5	b_2, -	0.5	b_4, -	2

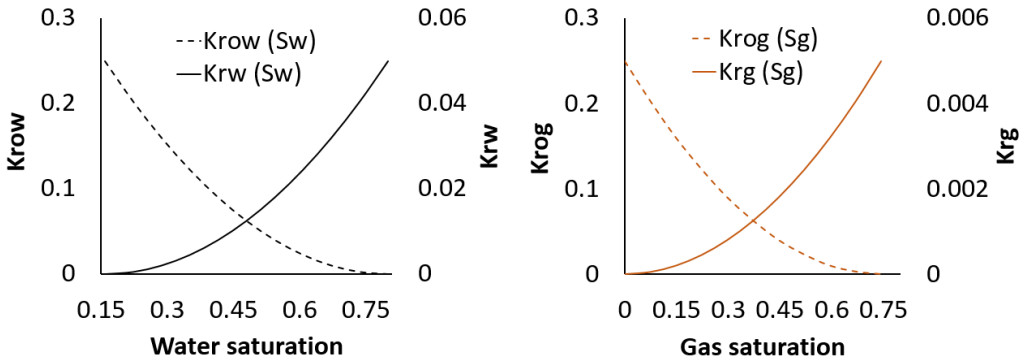

FIGURE 3. Input oil-water (left) and gas-oil (right) relative permeability functions.

4.2. **Role and scaling of heterogeneity.** In Figure 4 we present a vast set of simulation results within the constraints of the reference case (no gravity or hysteresis effects) with the following modifications: the uniform model 1 was run with r_w and $\lambda_w^{max}, \lambda_g^{max}$ being varied to generate values of M_{wag} over 2 orders of magnitude (black points). Each point indicates the simulated RF after 1.5 PVs injection of WAG (with water or gas injection as special cases) and the calculated mobility number. It is seen in Figure 4 (left, black points) that the variation in the stated input parameters induces a general trend where RF decreases from 0.80 at $M_{wag} = 1$ towards lower values when M_{wag} increases. The left part of Figure 4 also compares the Model 1 results with the same parameter cases run on Models 2-4 (non-black points) where heterogeneity is indicated by the parameter F_H increasing from 1 in Model 1 to 2.1, 3 and 12.9 in Models 2 to 4. Increased heterogeneity (higher F_H) generally lowers recovery since the phases flow preferentially in the high permeability layers, see Figure 5. Oil in the low permeable layers is recovered to less extent (high oil saturations close to initial values are seen by yellow color). The results were also plotted in Figure 4 (right) against M^* which under (only) these conditions equals $M_{wag}F_H$. By incorporating heterogeneity in the mobility number it is seen that the uniform and heterogeneous models scale to the same trend. Essentially, a higher M^* is obtained in a more heterogeneous reservoir which under base case conditions leads to lower RF.

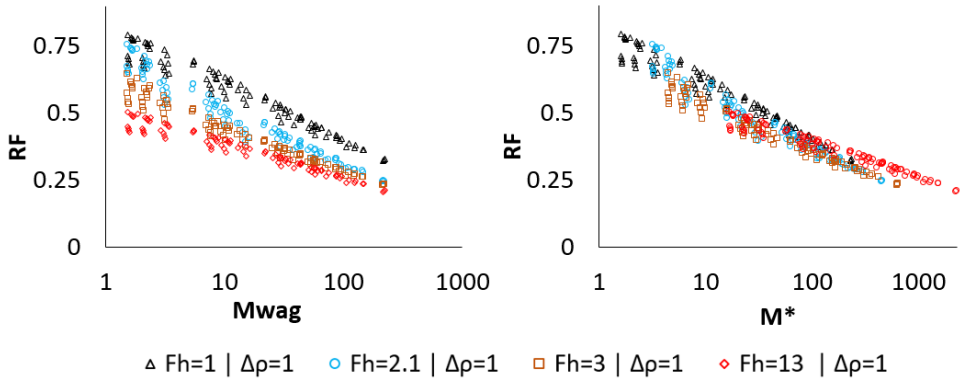

FIGURE 4. Scaling of RF data (after 1.5 PVs) under no-gravity no-hysteresis conditions by incorporating heterogeneity to approximate uniform model behavior. The results are plotted against M_{wag} (left) and M^* (right).

FIGURE 5. Oil saturation distribution in Model 4 ($F_H = 12.9$) after 1.5 PV of WAG injection with $r_w = 0.5$. Gravity and hysteresis effects are ignored.

4.3. **Gravity in uniform and layered models.** Next, the role of gravity was considered by comparing the $\Delta\rho = 1\text{kg/m}^3$ cases (negligible gravity) with corresponding simulations results using $\Delta\rho = 400\text{kg/m}^3$. The results are plotted against M_{wag} on the left side of Figure 6 using the four different models (F_H increasing down the rows of the figure). In the uniform model (row 1), the significant density difference leads to gravity segregation and poorer sweep. Hence, all simulations with high density difference get worse RF compared to their corresponding low density difference case. That effect is scaled by assigning values to the parameters a_1, a_2 in F_G (see (23) or (24) for $F_H = 1$). In essence, the mobility number is increased by a factor $F_G > 1$ to capture the worsened performance induced by the gravity mechanism.

At increased heterogeneity it is however observed that the two sets either have very comparable results (see row 2 in Figure 6 for $F_H = 2.1$) or higher RF (see row 3 and 4 for $F_H = 3$ and 12.9 in Figure 6) at high density difference $\Delta\rho$ compared to low $\Delta\rho$. In no-gravity cases with heterogeneity the flow occurs predominantly in the high permeable layers. However, when gravity becomes important the fluid density differences induce gas to rise and water to sink vertically and thus displacing oil in the low permeable layers along the way into the high permeable layers (see Figure 7). To account for this positive effect F_G was required to be less than 1 for high F_H, which is covered by the expression (24). The parameters a_1, a_2 were further tuned to give an overall match of both low and high F_H. The scaling formulation thus captures the interplay of gravity and heterogeneity effects for different flow regimes; in particular, that they isolated both have negative effects on recovery, but in combination have less negative impact. Essentially, gravity segregation appears to have potential of improving sweep in a heterogeneous reservoir. The scaled results are shown in the right side of Figure 6. Note that the difference between M_{wag} and M^* in this case is due to non-unity values of F_H and F_G.

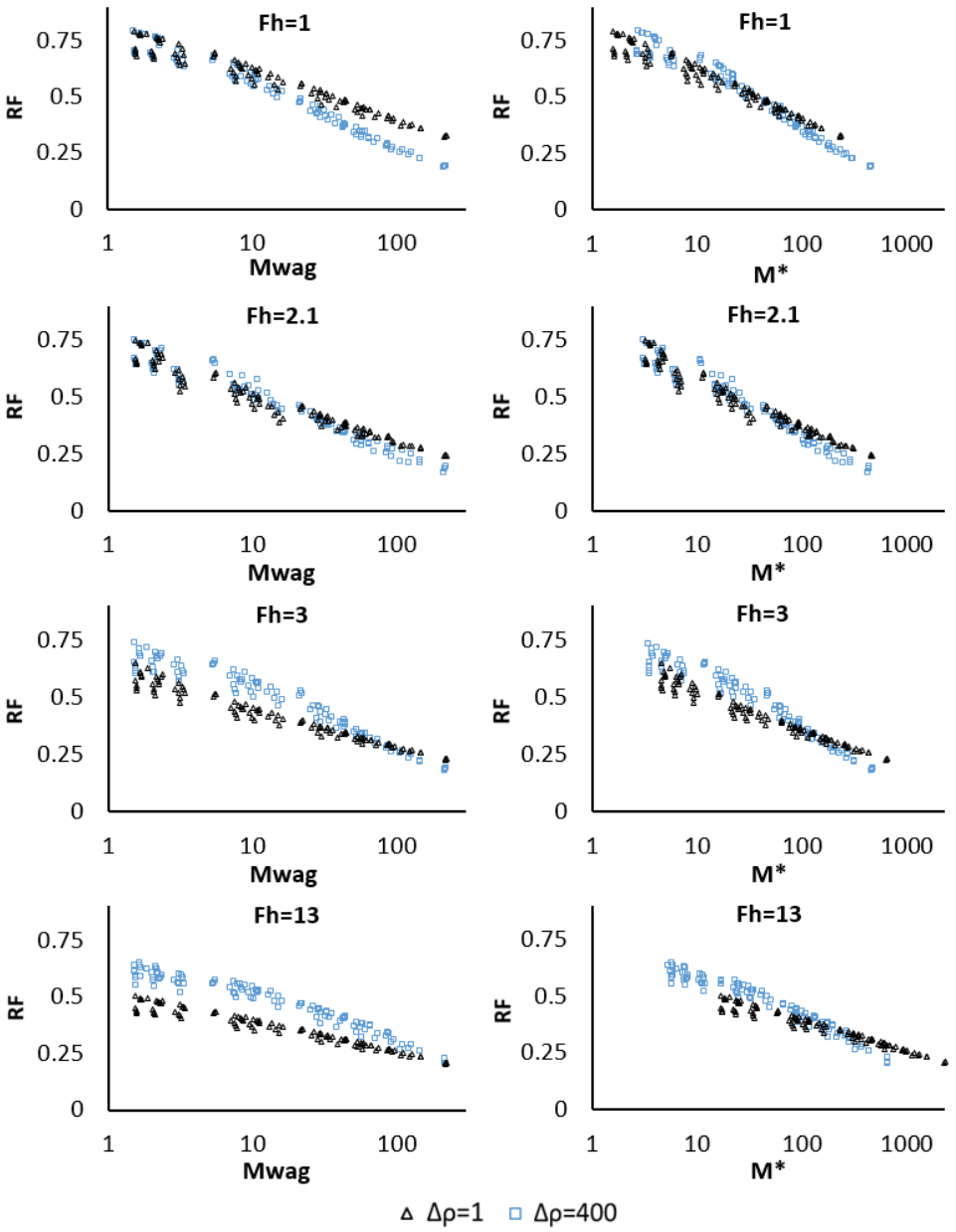

FIGURE 6. Scaling of RF data (after 1.5 PVs) for combined gravity and heterogeneity at no-hysteresis conditions. The results are plotted against M_{wag} (left) and M^* (right).

4.4. **Incorporation of hysteresis.** We here discuss the role and scaling of hysteresis effects in WAG injection. Hysteresis affects gas relative permeability and hence appears in $M^*_{g/o}$ and $N_G^{g/o}$. To separate these effects we first consider simulation results where gravity can be ignored by setting $\Delta\rho = 1$ kg/m^3 (very low) such that $N_G \approx 0$ and $F_G = 1$. Simulation results for the four models were then compared with and without hysteresis effects, as seen in Figure 8. As before, all four models are tested to account for heterogeneity at the same time. As seen in Figure 8 (left), the role of hysteresis under no-gravity conditions is similar for all the four models. RF is improved, which is expected when gas-to-oil mobility ratio becomes more favorable. We note that if $M^*_{g/o}$ is sufficiently reduced, then M^* will be reduced also, see (30), consistent with a formulation where lower M^* should correspond to higher RF. The parameters b_1, b_2 were thus tuned to give overlap

between the data. As seen in Figure 8 (right) the scaling is able to gather the results to excellent degree.

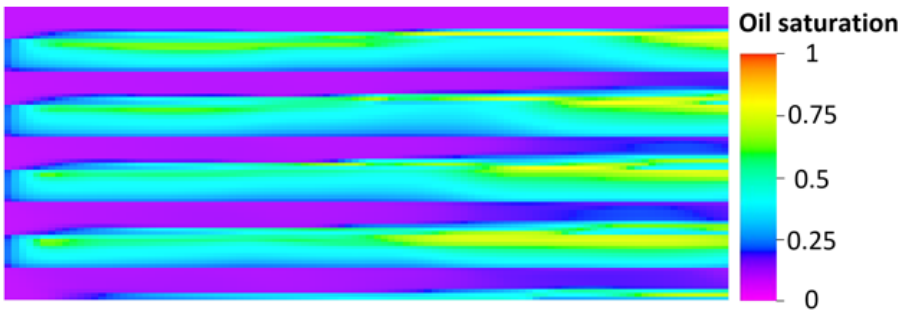

FIGURE 7. Oil saturation distribution in Model 4 ($F_H = 12.9$) after 1.5 PV of WAG injection with $r_w = 0.5$. Gravity improves recovery from low permeable layers. Hysteresis effects are ignored.

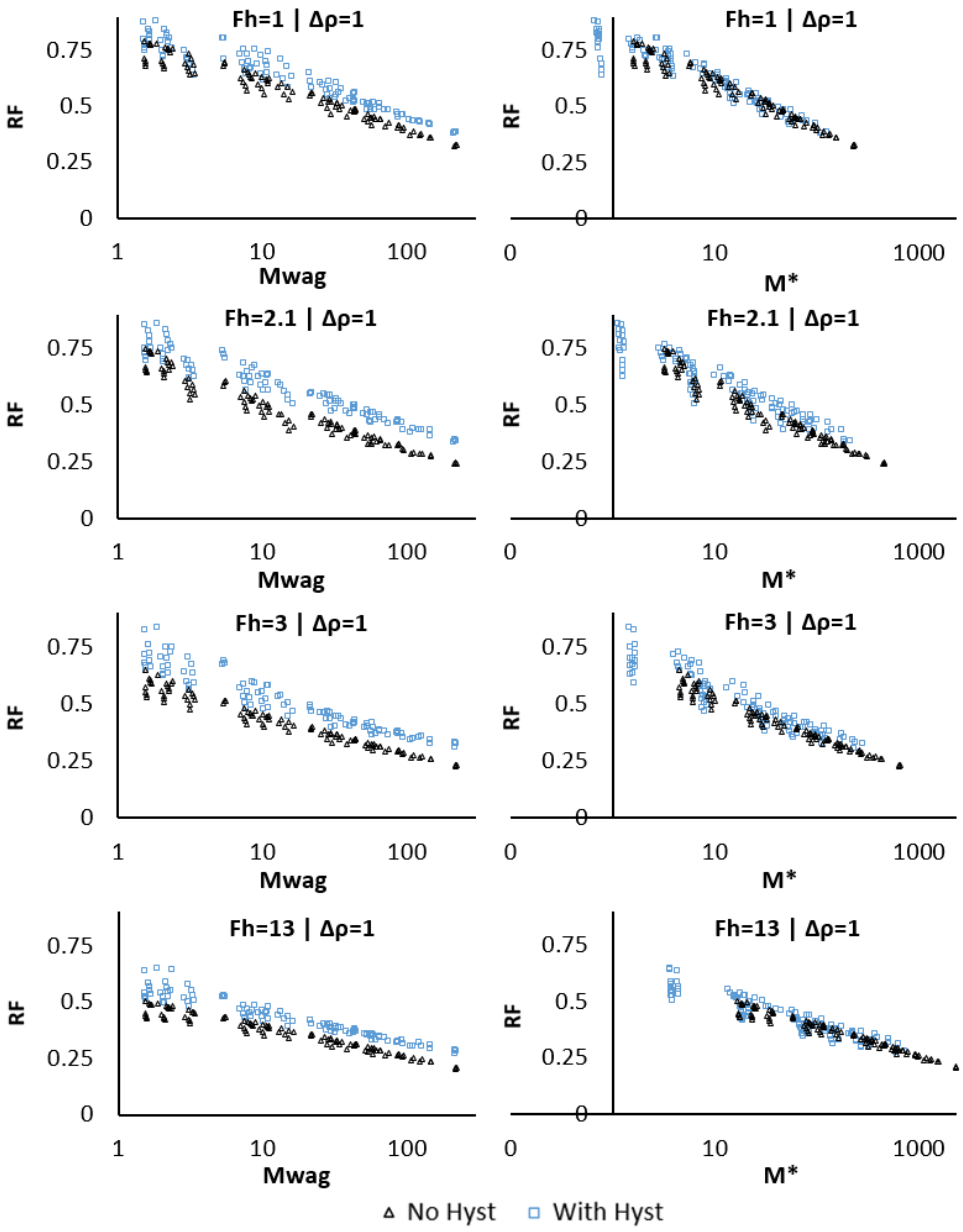

FIGURE 8. The role of hysteresis under no-gravity conditions. The results (RF after 1.5 PVs) are plotted against M_{wag} (left) and M^* (right).

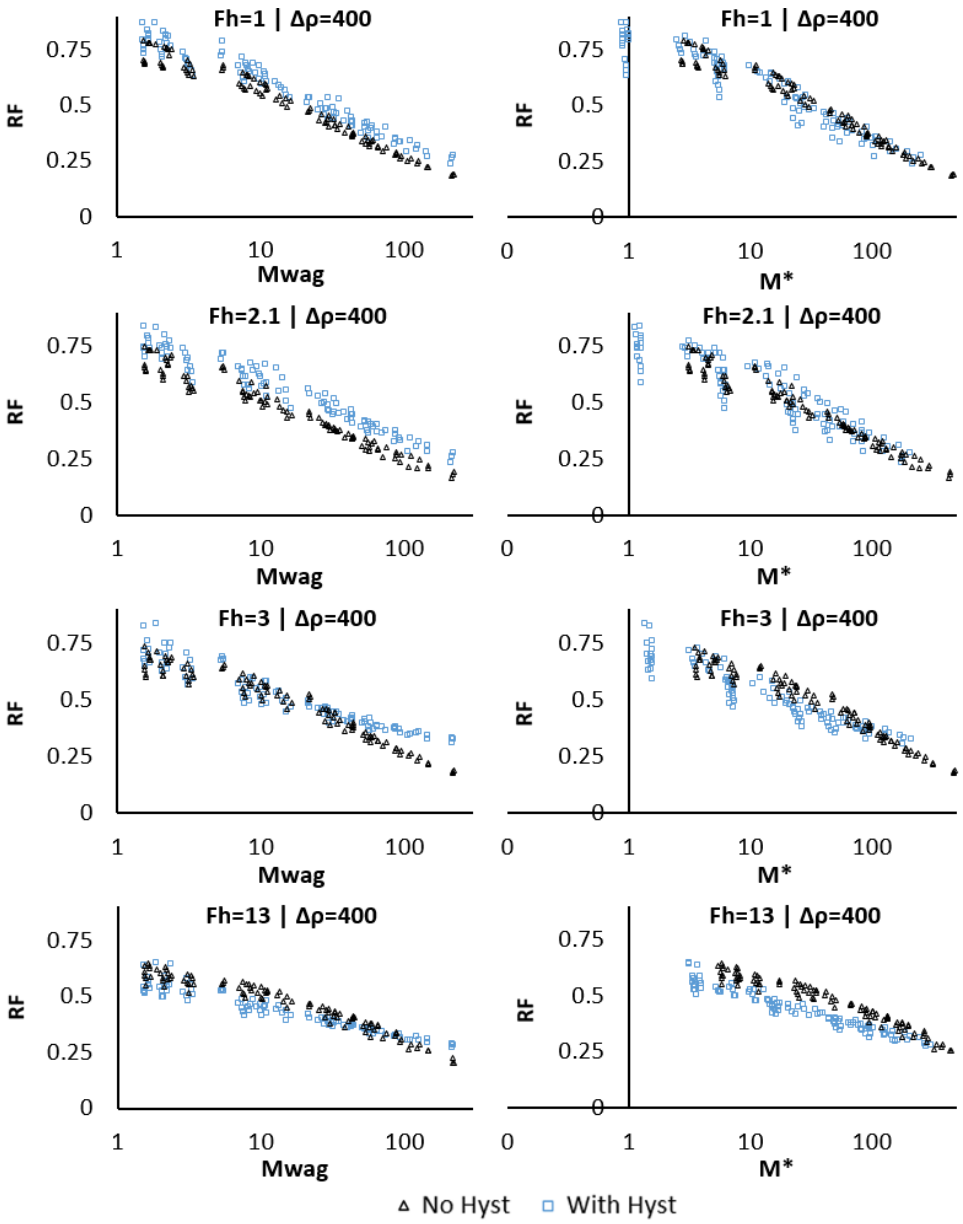

FIGURE 9. The role of hysteresis under gravity-influenced conditions. The results (RF after 1.5 PVs) are plotted against M_{wag} (left) and M^* (right).

Having determined the parameters controlling hysteresis in $M^*_{g/o}$ we now turn to a case where also gravity is a dominant factor. In Figure 9 the same simulations as just described are run, now only using $\Delta\rho = 400$ kg/m^3. For Model 1 and 2 (row 1 and 2) it is still seen that hysteresis contributes positively and increases the RF under otherwise identical conditions. Turning to the even more heterogeneous cases Model 3 and 4 it is however seen that the RF results are virtually identical or worse, respectively. Assuming the role of mobility ratio of gas to oil behaves as before, the change in performance should be related to gravity. As shown in Figure 7 gravity improves vertical sweep in heterogeneous reservoirs. At reduced gas mobility, gravitational flow is reduced and the positive effect on vertical sweep disappears. For the most heterogeneous model, it appears the loss of vertical sweep played a greater role than the improved mobility ratio. By tuning the parameters b_3, b_4 the results were adequately scaled as seen in Figure 9 (right). It is seen that in Model 3 and 4 the results appear more deviated after scaling than unscaled. However, one must

remember that this process compensates a reduction of M^* due to reduction of $M^*_{g/o}$ and shifts the data back to larger M^* as $F_G^{g/o}$ is increased towards 1.

4.5. **Optimal conditions for WAG.** In this section we systematically investigate the link between RF, M^* and r_w. Particularly, one of the key decisions during field production is the injection scheme. If WAG is to be considered as a better alternative than single phase injection (of water or gas) the model must predict the highest RF for a value of $0 < r_w < 1$ to support such a strategic decision. If RF is highest at $r_w = 0$ or 1, then gas or water injection should be preferred, respectively. For M^* to be a good measure of WAG performance it is also important to distinguish between these cases. Since high values of M^* are linked to lower RF we require M^* to show opposite trends with r_w as RF, e.g. if RF has a central peak vs r_w, then M^* should have a minimum at a similar value of r_w. Also, if RF increases / decreases with r_w then M^* should decrease / increase with r_w.

A representative selection of the previously presented simulations are sorted in Figures 10 (cases without hysteresis) and 11 (corresponding cases with hysteresis) where both RF and M^* are plotted against r_w from 0 to 1. As can be seen from the legend, the upper two rows consider Model 1 (uniform) without gravity (row 1) and with gravity(row 2). The same for Model 4 (strongly heterogeneous) is shown in row 3 and 4. Column 1 to 3 applies parameter pairs $(\lambda_w^{max}, \lambda_g^{max}) = (1,1); (1,10); (10,10)$ in units cP^{-1}. As stated in the base case, $\lambda_{ow}^{max} = \lambda_{og}^{max} = 1$ cP^{-1} was applied for the oil phase.

Figure 10 shows the expected correspondence between trends vs r_w for RF and M^* in most cases. In column 2 the trends are monotonous and opposite as they should be. These cases consider high gas mobility compared to water (M^* is ca an order of magnitude higher at $r_w = 0$ compared to at $r_w = 1$). It is well captured that both parameters change quickly at low r_w and then slowly or stabilize at high r_w. Due to the mathematical formulation of M^* as function of r_w a monotonous relation will always be the case when hysteresis is not involved. That is seen in all cases of Figure 10. As a consequence it also follows that when M^* is the same for $r_w = 0$ as for $r_w = 1$, then M^* is constant. That is seen in column 1 and 3 where gas and water have identical mobility parameters. Essentially the injection fluids should have identical displacement behavior relative to oil, but due to gravity they will cover opposite vertical parts of the reservoir. In agreement with the constant M^* most of the cases in column 1 and 3 also display a constant or very weak dependence of RF with r_w. However, in some cases (columns 1 and 3 on rows 1 and 4) it is seen that RF has a central peak while M^* is constant. It is possible that in situations where both water and gas flow through same paths (in low-gravity or strong heterogeneity cases), their presence will reduce each others mobility leading to improved mobility ratio to oil for both injected phases. By similar reasoning, reduced injectivity may occur for either injected phases during WAG injection, as water and gas are competing for the same pore space (Fager et al., 2019). Such mobility reduction would depend on r_w since a high saturation and high mobility of the displacing fluid would be obtained behind the front otherwise. Such a mechanism is currently not incorporated in the scaling number M^*.

Figure 11 shows the simulation results where hysteresis is activated plotted against r_w. In column 1 and 3 it is seen that WAG is favorable over single phase injection in all cases as displayed by a strong (or small) peak in RF vs r_w. These trends are captured symmetrically by M^* in all these cases (column 1 and 3), also with magnitude of variation that of RF in most cases. In column 2 one of four cases favors WAG injection (weakly), while the other three show similar RF for central and high r_w. The latter trend is captured by M^* whereby a high M^* is shown at $r_w = 0$ while lower and similar values are shown for central and high r_w. The one favorable WAG case has an overall symmetric trend with M^* except for the last point. In essence, the M^* formulation strongly captures the trends in RF vs r_w when hysteresis is involved.

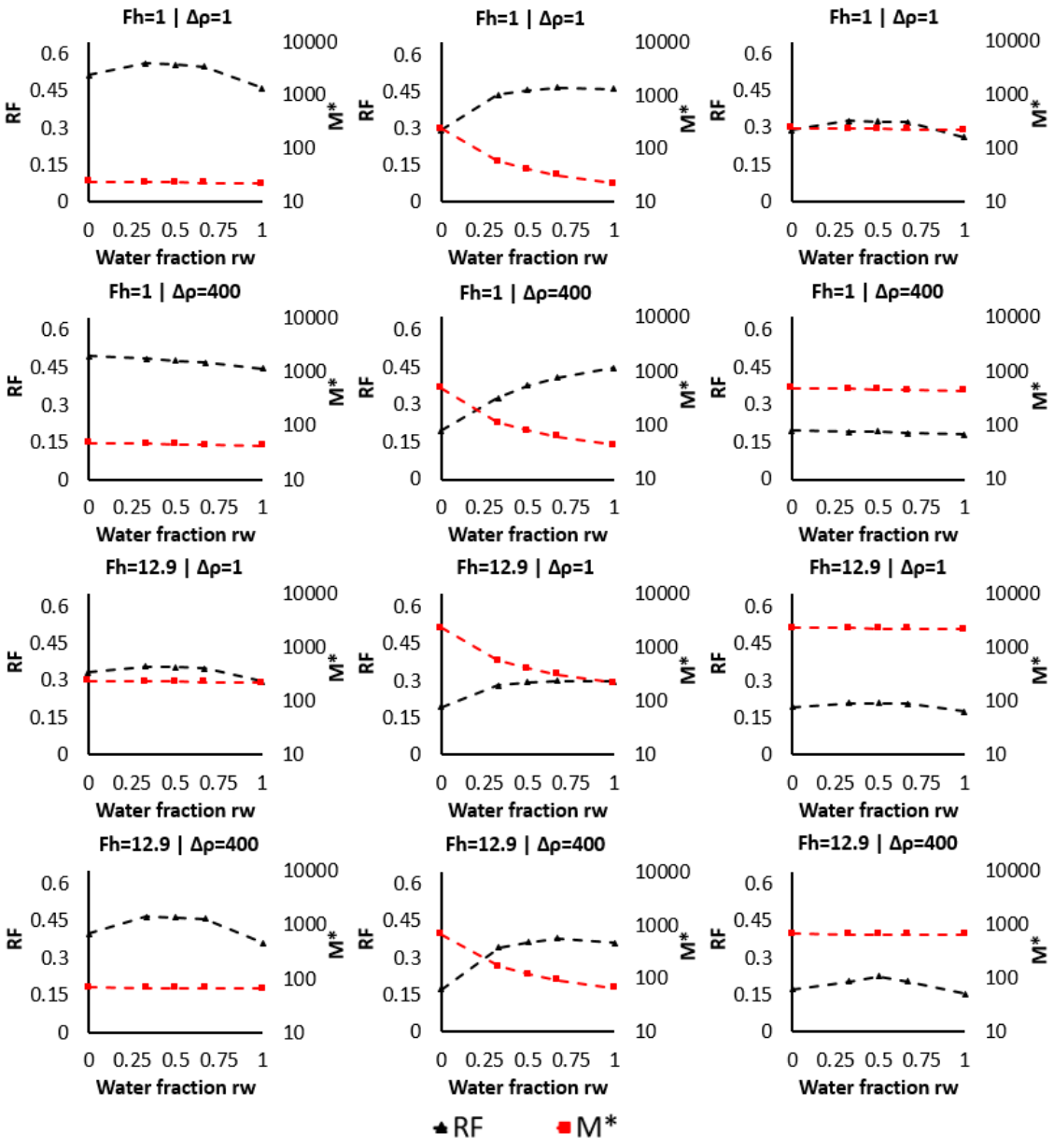

FIGURE 10. Relations RF vs r_w (black points) and M^* vs r_w (red points) for Model 1 (row 1 and 2) and Model 4 (row 3 and 4), with and without gravity. Column 1 to 3 applies $(\lambda_w^{max}, \lambda_g^{max}) = (1,1); (1,10); (10,10)$ [cP^{-1}]. Hysteresis was not applied in any of these simulation tests.

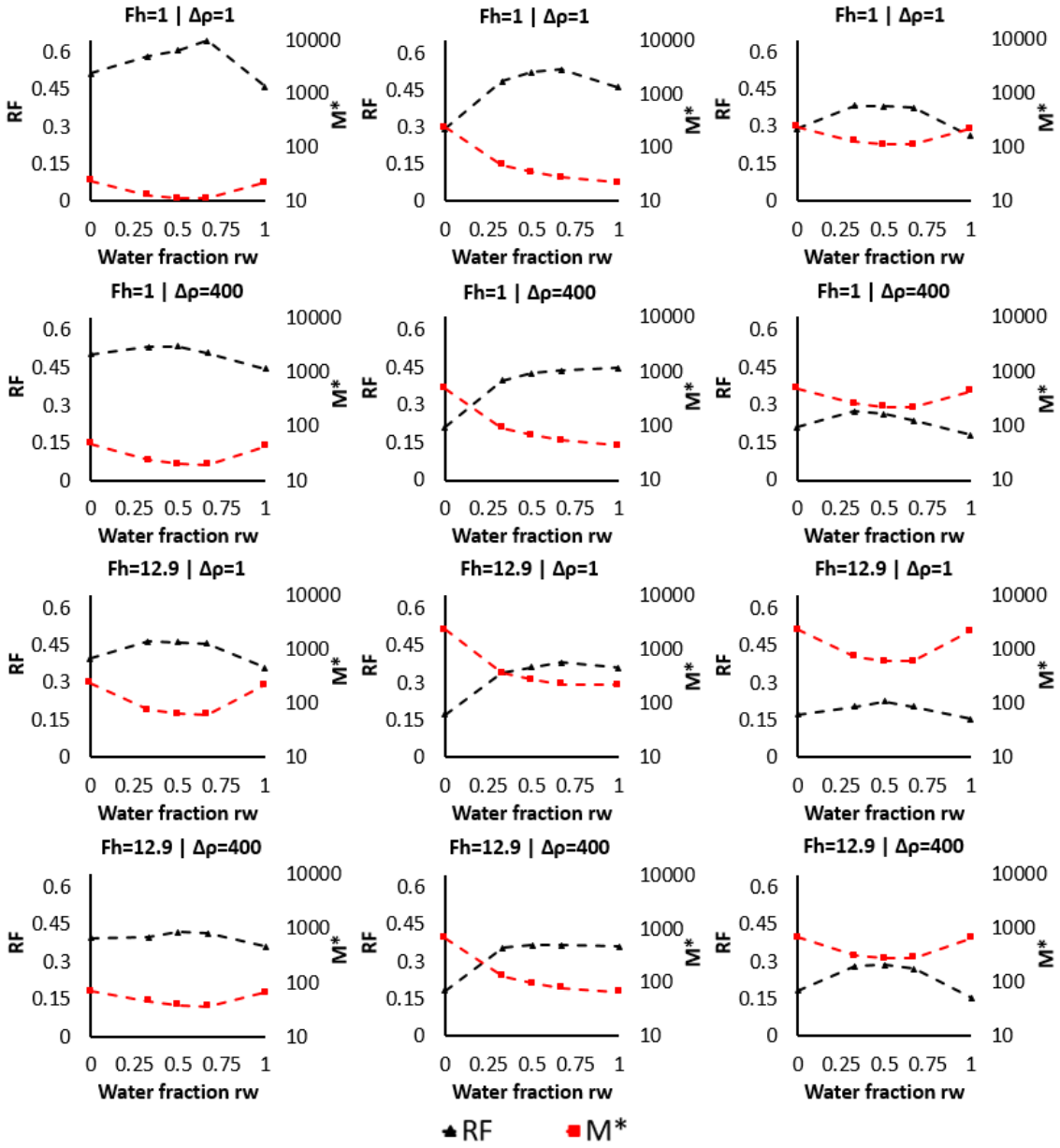

FIGURE 11. Relations RF vs r_w (black points) and M^* vs r_w (red points) for Model 1 (row 1 and 2) and Model 4 (row 3 and 4), with and without gravity. Column 1 to 3 applies $(\lambda_w^{max}, \lambda_g^{max}) = (1,1); (1,10); (10,10)$ [cP^{-1}]. Hysteresis was applied in all of these simulation tests.

4.6. **Overall scaling of results.** To summarize, we have gathered all the simulation results into Figure 12, and plotted RF against corresponding values of M_{wag} (left) and M^* (right). Since M_{wag} does not account for heterogeneity, gravity or hysteresis, there is great variation in RF for a given value of M_{wag} (a range of 0.40 for $M_{wag} \approx 1$ and a range of 0.20 for $M_{wag} \approx 100$). When the same data are plotted vs M^*, where these effects are accounted for, it is noted that the data are much more collected, now with a range between 0.15 and 0.25. The values of M^* cover three orders of magnitude (while the original values of M_{wag} cover two) indicating the shift along the axis to compensate for the stated effects. It should be noted that the scaling was done

manually and mechanism by mechanism rather than making a systematic minimization of the overall scatter.

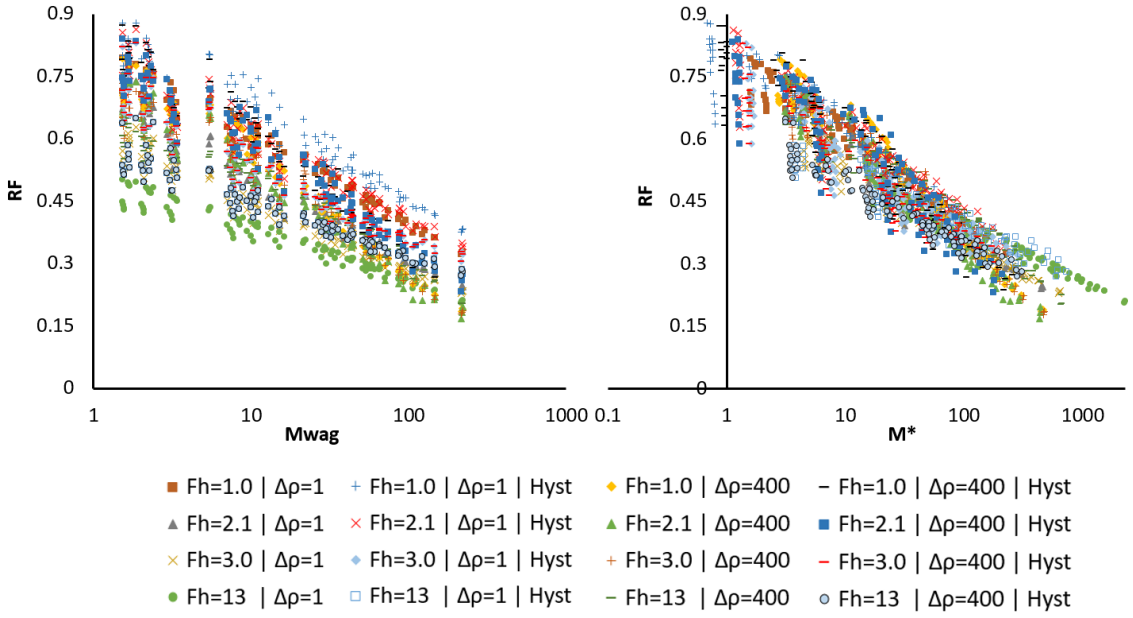

FIGURE 12. Overview of all simulation results plotted vs M_{wag} (left) and M^* (right).

4.7. **Limitations and extensions.** One of the mechanisms not considered in detail was capillary pressure. Its effect typically diminishes with higher permeability, larger dimensional scale (in our case the height of the low permeable layers) and high velocity. In low permeable, densely fractured reservoirs it can however be a main drive mechanism for production (Andersen, 2019). Its role was evaluated by implementing two phase curves P_{cow}, P_{cgo} from water-wet Berea sandstone (Larsen et al., 2000; Kantzas et al., 1998), rescaled by Leverett Bear (2013) assumptions to J_{ow}, J_{go}:

$$P_{cgo} = \sigma_{go}\sqrt{\phi/K_x}J_{go}, \qquad P_{cgo} = \sigma_{ow}\sqrt{\phi/K_x}J_{ow}. \tag{32}$$

where σ_{go}, σ_{ow} denote gas-oil and oil-water interfacial tensions. The curves, shown in Figure 13, display water-wetness over oil and oil-wetness over gas. Hence, capillary forces improve displacement of oil by water, but hinder displacement of oil by gas. Overall, that can give increased or decreased oil recovery compared to not considering capillary forces, depending on which mechanism is more dominant.

The impact on oil recovery vs time is seen in Figure 14. It was found that capillary pressure played a second order role in most or all cases, although it had a positive effect on recovery in the most heterogeneous systems (e.g. Model 4) where also the lowest permeabilities were considered. This also indicates that capillary pressure induced crossflow may improve vertical sweep in heterogeneous systems subject to hysteresis, see also Afzali et al. (2018). In oil-wet formations, capillary forces could prevent both water and gas from entering the low permeable layers. It must be emphasized that a proper accountancy of capillary forces during WAG would require initializing the saturation distribution accordingly and incorporate hysteresis relations also for these functions.

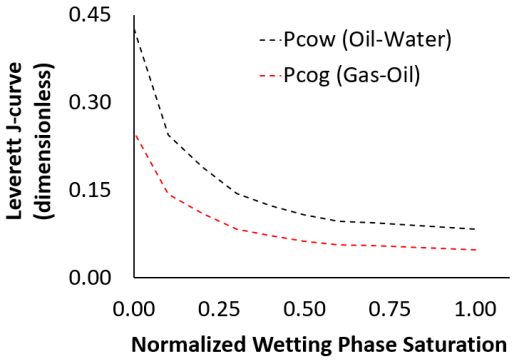

FIGURE 13. Scaled oil-water and gas-oil capillary pressure functions plotted against normalized wetting phase saturations. Based on Larsen et al. (2000); Kantzas et al. (1998) for water-wet Berea sandstone.

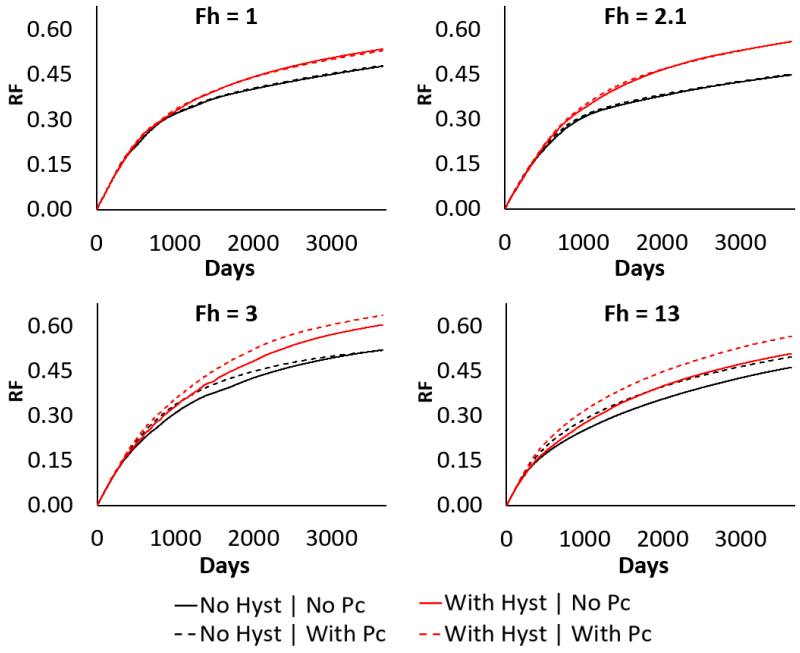

FIGURE 14. Sensitivity to capillary pressure for the base case with WAG injection ($r_w = 0.5$) and gravity ($\Delta\rho = 400$ kg/m^3) effects.

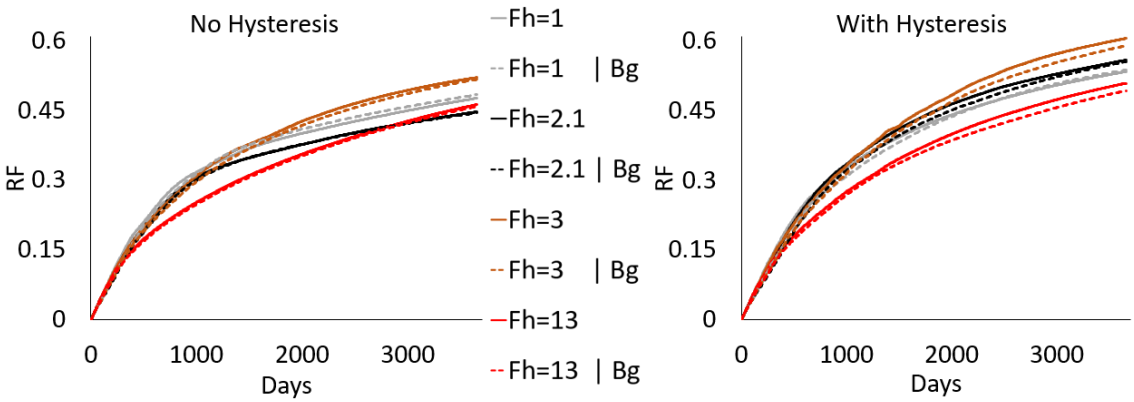

FIGURE 15. Sensitivity to gas compressibility, by gas formation volumetric factor (B_g) as given in (33), for the base case with WAG injection ($r_w = 0.5$) and gravity ($\Delta\rho = 400$ kg/m^3) effects.

Fluid compressibility was briefly investigated for the gas phase where a non-constant volume factor B_g (33) was used to represent ideal gas behavior (Standing and Katz, 1942).

$$B_g = \frac{\rho_g(P)}{\rho_g(P_{init})} = \frac{P_{init}}{P}. \tag{33}$$

In Figure 15 the impact of this (marked B_g) is compared to the base assumption of a constant gas density. Mainly, the differences are negligible, although some impact on recovery is found when hysteresis is included and F_h is large. The effect of compressibility may be positive on oil recovery, with improved crossflow and expulsion of oil from low permeable reservoir regions (Surguchev et al., 1992). It might also be negative, where a lower effective gas slug size and a pressure dampening effect (Stenger et al., 2011) would likely further increase the F_h-dependent channelling effects (Al-Bayati et al., 2019). Combined, these mechanisms may explain the near-indifferent effects or apparently non-systematic effect on recovery.

Other aspects not addressed are the cycle frequency (how often injection fluid is switched), hysteresis of water or oil, gas solubility and that the reservoir may be inclined, i.e. with layers not directly normal to the gravitational field. During injection, the reservoir pressure distribution is more stable compared to a depletion scenario. Also considering that the highest pressure variations are near the wells, we can consider pressure effects on density to be of less importance. The densities implemented into the model should hence be considered as characteristic average values for the relevant reservoir conditions. Namani and Kleppe (2011) found that, with the half-cycles of both phases equal, doubling or halving them did not yield any difference in oil recovery. Studies by Chen and Reynolds (2016) and Mirkalaei et al. (2011) could however indicate some impact.

Considering that this is a scaling study, some limitations of the scope were selected to reduce the system complexity. We do however believe that the main mechanisms are captured, namely advection, gravity, heterogeneity, hysteresis and their interplay. As such, the proposed scaling number can indicate trends in recovery. The considered approach does naturally extend to incorporate other model assumptions. For example, hysteresis in oil or water can be scaled in a similar way as assumed for gas, by correlating the characteristic mobility parameters with hysteresis model parameters. The use of the Land and Carlson models are not restrictions of our model, but examples of how hysteresis can be incorporated.

A benefit obtained from the scaling is that the model can be applied to effectively estimate performance of a reservoir without running time demanding simulations. Especially, if there is uncertainty in fluid properties, geometrical properties or saturation functions, the model can be used to quickly assess how this uncertainty is reflected in the range of M^* values and corresponding recovery performance. For a given base case reservoir model it is also expected that the scaling

can assist in selecting favorable WAG cases before running long term field scale simulations. Scaling studies frequently rely on the assumption of homogeneous systems with few mechanisms at play. The proposed methodology provides a systematic approach of dealing with WAG and possibly other complex EOR methods in heterogeneous settings. Beyond the scope of this study, the presented results could be applied as a baseline pool of data from which comparisons to sequentially more complex systems can be made. This might involve evaluation of other relative permeability hysteresis models, fluid compressibility and capillary pressure which could be studied with regards to the compound influence from mobility, heterogeneity, gravity and hysteresis.

5. Conclusions

In this paper a simulation study was performed where WAG injection was conducted in a horizontally layered reservoir. Reservoir heterogeneity, gas-water volume injection fractions, fluid mobilities, gravity segregation (driven by density differences) and hysteresis effects were studied. Characteristic time scales (for residence and gravity segregation), dimensionless numbers (gravity number N_G and mobility ratio M) and multipliers (F_H for heterogeneity and F_G for gravity) were defined based on the physical processes taking place and their interplay to integrate all these effects into a single dimensionless mobility number, termed M^*. The following trends in model behavior were found:

- In uniform models, gravity led to segregation and lower RF. For the no-gravity models RF declined with increases in heterogeneity.
- In heterogeneous models, gravity was a positive mechanisms compared to no-gravity cases as injection fluids were diverted into low-permeable layers giving higher RF.
- Hysteresis lowers gas mobility and hence improves gas-oil mobility ratio and reduces gravity segregation. The first effect is always positive, but the second is mainly positive in more uniform reservoirs where gravity segregation has a negative effect on recovery. In heterogeneous reservoirs, reducing gravity segregation can lead to that the oil in low permeable layers remains unswept.
- Without hysteresis built into the model, single-phase injection was preferred in most cases. This makes it important to perform laboratory measurements to evaluate gas mobility, entrapment and related hysteretic response, when evaluating the potential for WAG injection in a real field
- With hysteresis present, WAG could supercede recovery over single-phase injection by significant margin in most of the studied cases.
- It is important to investigate the interplay between gravity and hysteresis on optimization procedures for WAG, as these were observed to have differing impacts on recovery individually than when combined.

The proposed scaling number M^* was used to scale the results. The following observations were made:

- WAG performance can be characterized by just one dimensionless number, M^*. Accordingly RF can be predicted just knowing M^* and the impact of model input parameters on RF can be directly associated with how they affect M^*.
- The scaling number accounts for water-oil and gas-oil mobility ratio, reservoir heterogeneity, gravity effects from both water and gas phases, relative permeability hysteresis, and the applied WAG ratios.
- The trends in recovery explained above are captured by symmetrical trends in M^* where a higher value of M^* results in lower recovery factor.

Acknowledgments

The authors acknowledge the Research Council of Norway and the industry partners, ConocoPhillips Skandinavia AS, Aker BP ASA, Eni Norge AS, Equinor ASA, Neptune Energy Norge AS, Lundin Norway AS, Halliburton AS, Schlumberger Norge AS, Wintershall Norge AS, and DEA Norge AS, of The National IOR Centre of Norway for support. We also thank Kenny Walrond for early simulation work.

Nomenclature

Roman.

B_g	=	Gas formation volume factor
C	=	Lands's trapping parameter, -
f_i	=	Fractional flow function, -
F_H	=	Heterogeneity multiplier, -
F_G	=	Gravity multiplier, -
h_j	=	Layer height, m
J_{wo}, J_{go}	=	Scaled capillary pressure, -
k_{ri}	=	Relative permeability, -
k_{ri}^{max}	=	Relative permeability end points, -
K_x, K_z	=	Horizontal and vertical absolute permeability, m^2
L_x	=	Distance from injector to producer, m
L_y	=	Width of reservoir, m
L_z	=	Total height of reservoir, m
M	=	Mobility ratio, -
M_{WAG}	=	Simple characteristic three phase mobility ratio, -
M^*	=	Universal characteristic three phase mobility ratio, -
n_i	=	Corey exponents, -
N_G	=	Gravity number, -
P_c	=	Capillary pressure, Pa
p_i	=	Phase pressure, Pa
r_w	=	Water volume fraction in a WAG cycle, -
s_{ir}	=	Residual phase saturation
s_i	=	Local phase saturation, -
S_i	=	Normalized saturation, -
t	=	Time, s
T^{g-hc}	=	Gas half-cycle time, s
T^{w-hc}	=	Water half-cycle time, s
T^{tot}	=	Total injection time, s
u_i	=	Darcy phase velocity, m/s
u_T	=	Total Darcy velocity, m/s
x	=	Horizontal direction towards producer, m
z	=	Vertical direction downwards, m

Greek.

α	=	Hysteresis parameter, -
$\Delta\rho$	=	Density difference, kg/m^3
λ_i	=	Phase mobility, $(Pa{\cdot}s)^{-1}$
μ_i	=	Phase viscosity, Pa·s
ρ_i	=	Phase density, kg/m^3
σ_{ow}, σ_{go}	=	Interfacial tension, N/m
τ	=	Time scale, s
ϕ	=	Porosity, -

Indices.

$*$	=	Characteristic value
$1pv$	=	1 pore volume
$arit$	=	Arithmetic
g	=	Gas
G	=	Gravity
$harm$	=	Harmonic
i	=	Phase
j	=	Layer
o	=	Oil
res	=	Residence
$init$	=	Initial reservoir condition
seg	=	Segregation
T	=	Total
w	=	Water

References

Afzali, S., Rezaei, N., and Zendehboudi, S. (2018). A comprehensive review on enhanced oil recovery by water alternating gas (wag) injection. *Fuel*, 227.

Ahmed Elfeel, M., Al-Dhahli, A., Jiang, Z., Geiger, S., van Dijke, M. I., et al. (2013). Effect of rock and wettability heterogeneity on the efficiency of wag flooding in carbonate reservoirs. In *SPE Reservoir Characterization and Simulation Conference and Exhibition*.

Al-Bayati, D., Saeedi, A., Myers, M., White, C., and Xie, Q. (2019). An experimental investigation of immiscible-co2-flooding efficiency in sandstone reservoirs: Influence of permeability heterogeneity. *SPE Reservoir Evaluation & Engineering*, 22(03):990–997.

Alzayer, H. and Sohrabi, M. (2018). *SPE-190346-MS*, chapter Water-Alternating-Gas Injection Simulation - Best Practices, page 9. Society of Petroleum Engineers, Muscat, Oman.

Andersen, P. Ø. (2019). A simplified modelling approach for petroleum recovery by spontaneous imbibition in naturally fractured reservoirs. *Journal of Natural Gas Science and Engineering*, 63:95 – 114.

Baojun, F., Xingjia, D., and Cai, Y. (1997). Pilot test of water alternating gas injection in heterogeneous thick reservoir of positive rhythm sedimentation of daqing oil field. *SPE Advanced Technology Series*, 5(01):41–48.

Bear, J. (2013). *Dynamics of fluids in porous media*. Courier Corporation.

Brooks, R. and Corey, A. (1964). Hydraulic properties of porous media. *Hydrology Papers, Colorado State University*.

Buckley, S. E. and Leverett, M. (1942). Mechanism of fluid displacement in sands. *Transactions of the AIME*, 146(01):107–116.

Carlson, F. M. (1981). Simulation of relative permeability hysteresis to the nonwetting phase. In *SPE Annual Technical Conference and Exhibition*.

Chen, B. and Reynolds, A. C. (2016). Ensemble-based optimization of the water-alternating-gas-injection process. *SPE Journal*, 21(03):786–798.

Chen, Z., Huan, G., and Ma, Y. (2006). *Computational methods for multiphase flows in porous media*. SIAM.

Christensen, J. R., Stenby, E. H., and Skauge, A. (2001). Review of wag field experience. *SPE Reservoir Evaluation & Engineering*, 4(02):97–106.

Craig Jr, F., Geffen, T., and Morse, R. (1955). Oil recovery performance of pattern gas or water injection operations from model tests. *Petroleum Transactions AIME*, 204:7–15.

Fager, A., Crouse, B., Sun, G., Xu, R., and Freed, D. (2019). *SPE-195734-MS*, chapter Evaluation of Directly Simulated WAG Hysteresis at Pore Scale and its Effect on Injectivity Index, page 12. Society of Petroleum Engineers, Aberdeen, UK.

Fatemi, S. M., Sohrabi, M., et al. (2012). Experimental and theoretical investigation of water/gas relative permeability hysteresis: applicable to water alternating gas (wag) injection and gas storage processes. In *Abu Dhabi International Petroleum Conference and Exhibition*.

Geffen, T. M., Owens, W. W., Parrish, D. R., and Morse, R. A. (1951). Experimental investigation of factors affecting laboratory relative permeability measurements. *Journal of Petroleum Technology*, 3(04):99–110.

Genrich, J. et al. (1986). A simplified model to predict heterogeneity effects on wag flooding performance. In *SPE Annual Technical Conference and Exhibition*. Society of Petroleum Engineers.

GeoQuest (2014). Eclipse 100: Reference manual and technical description. *Schlumberger*.

Habermann, B. (1960). The efficiency of miscible displacement as a function of mobility ratio. *Petroleum Transactions AIME*, 219:264–272.

Hagoort, J. (1980). Oil recovery by gravity drainage. *SPE Journal*, 20(03):139–150.

Hoare, G., Coll, C., et al. (2018). Effect of small/medium scale reservoir heterogeneity on the effectiveness of water, gas and water alternating gas wag injection. In *SPE Europec featured at 80th EAGE Conference and Exhibition*.

Hoseini, J., Masoudi, R., Mousavi Mirkalaei, S. M., Ataei, A., and Demiral, B. (2011). *IPTC-15055-MS*, chapter Investigating the Effect of Hysteresis modelling on Numerical Simulation of Immiscible WAG Injection, page 17. International Petroleum Technology Conference, Bangkok, Thailand.

Kamali, F., Hussain, F., and Cinar, Y. (2017). An experimental and numerical analysis of water-alternating-gas and simultaneous-water-and-gas displacements for carbon dioxide enhanced oil recovery and storage. *SPE Journal*, 22(02):521–538.

Kantzas, A., Nikakhtar, B., Pow, M., et al. (1998). Principles of three phase capillary pressures. *Journal of Canadian Petroleum Technology*, 37(07).

Khorsandi, S., Li, L., and Johns, R. T. (2017). Equation of state for relative permeability, including hysteresis and wettability alteration. *SPE Journal*, 22(06):1915–1928.

Kumar, J., Agrawal, P., and Draoui, E. (2017). A case study on miscible and immiscible gas-injection pilots in a middle east carbonate reservoir in an offshore environment. *SPE Reservoir Evaluation & Engineering*, 20(01):19–29.

Land, C. S. (1968). Calculation of imbibition relative permeability for two- and three-phase flow from rock properties. *SPE Journal*, 8(02):149–156.

Larsen, J. A., Thorsen, T., and Haaskjold, G. (2000). Capillary transition zones from a core analysis perspective. In *SCA Annual Symposium*.

Mirkalaei, M., Mousa, S., Hoseini, J., Masoudi, R., Ataei, A., Demiral, B., Karkooti, H., et al. (2011). Investigation of different i-wag schemes toward optimization of displacement efficiency. In *SPE Enhanced Oil Recovery Conference*.

Moreno, J. E. and Flew, S. (2011). *SPE-143568-MS*, chapter EOR: Challenges of Translating Fine Scale Displacement into Full Field Models, page 14. Society of Petroleum Engineers, Kuala Lumpur, Malaysia.

Namani, M. and Kleppe, J. (2011). Investigation of the effect of some parameters in miscible wag process using black-oil and compositional simulators. In *SPE Enhanced Oil Recovery Conference*.

Namani, M., Souraki, Y., Kleppe, J., Høier, L., and Karimaie, H. (2017). Scaled experimental and simulation study of segregation in water-above-gas injection. *SPE Reservoir Evaluation & Engineering*, 20(04):809–819.

Pal, M., Pedersen, R. B., Gilani, S. F., and Tarsauliya, G. (2018). *SPE-190343-MS*, chapter Challenges and Learnings from Operating the Largest Off-Shore WAG in the Giant Al-Shaheen Field and Ways to Optimize Future WAG Developments, page 25. Society of Petroleum Engineers, Muscat, Oman.

Righi, E. F., Royo, J., Gentil, P., Castelo, R., Del Monte, A., and Bosco, S. (2004). *SPE-89360-MS*, chapter Experimental Study of Tertiary Immiscible WAG Injection, page 10. Society of Petroleum Engineers, Tulsa, Oklahoma.

Sedaghat, M. H. and Azizmohammadi, S. (2018). Representative-elementary-volume analysis of two-phase flow in layered rocks. *SPE Reservoir Evaluation & Engineering (preprint)*, page 9.

Sedaralit, M. F., Hashim, N., Mandal, D., et al. (2016). Translating a robust techniques of the eor-wag hysteresis from laboratory to field application. In *International Petroleum Technology Conference*. International Petroleum Technology Conference.

Shahverdi, H. and Sohrabi, M. (2014). Modeling of cyclic hysteresis of three-phase relative permeability during water-alternating-gas injection. *SPE Journal*, 20(01):35–48.

Shahverdi, H. and Sohrabi, M. (2016). Relative permeability characterization for water-alternating-gas injection in oil reservoirs. *SPE Journal*, 21(03):799–808.

Standing, M. B. and Katz, D. L. (1942). Density of natural gases. *Transactions of the AIME*, 146(01):140–149.

Stenger, B. A., Al Kendi, S. A., Al Katheeri, A. B., and Al Ameri, A. F. (2011). Interpretation of immiscible wag repeat pressure-falloff tests. *SPE Reservoir Evaluation & Engineering*, 14(06):687–701.

Surguchev, L., Korbol, R., Haugen, S., Krakstad, O., et al. (1992). Screening of wag injection strategies for heterogeneous reservoirs. In *European petroleum conference*. Society of Petroleum Engineers.

Talabi, O. A., Moreno, J. E., Malhotra, R. K., and Tham, B. K. (2019). *SPE-194634-MS*, chapter Practical Upscaling of Immiscible WAG Hysteresis Parameters from Core to Full Field Scale, page 17. Society of Petroleum Engineers, Mumbai, India.

van Lingen, P. P., Barzanji, O. H. M., and van Kruijsdijk, C. P. J. W. (1996). *SPE-36662-MS*, chapter WAG Injection to Reduce Capillary Entrapment in Small-Scale Heterogeneities, page 7. Society of Petroleum Engineers, Denver, Colorado.

Xia, D.-F., Xu, S.-L., and Qi, F. (1999). A proof of the arithmetic mean-geometric mean-harmonic mean inequalities. *RGMIA research report collection*, 2(1).

6. Author biographies

Jan Inge Nygård (26) is Consultant at Bouvet Norge AS, division Bouvet Stavanger in Norway. He holds MSc in Petroleum Technology from University of Stavanger, Norway. He has co-authored one conference paper. His research relates to numerical simulation work into Water-Alternating-Gas (WAG) processes.

Pål Ø. Andersen (35) is Associate Professor in Reservoir Technology at the University of Stavanger, Norway and the National IOR Centre of Norway and holds PhD in Petroleum Technology. He has co-authored 40+ technical papers, reviewed 100 technical papers and serves as Managing Guest Editor in Journal of Natural Gas Science & Engineering. His research relates to flow in porous media, enhanced oil and gas recovery, CCUS, SCAL, shale gas production and naturally fractured reservoirs.

Appendix A. Scaling recovery during twophase advective displacement

Let S be normalized water saturation, x be scaled length so that $x = 1$ at the producer and time be measured in volumes of mobile oil (denoted 1 mobile pore volume MPV) so that at $t = 1$ a perfect displacement has produced all the mobile oil. The water fractional flow function is:

$$f_w(S) = \frac{M}{1+M}, \tag{34}$$

Assume Buckley Leverett displacement. After 1 MPV ($t = 1$)the front has either reached or passed the producer. The saturation at the producer $x = 1$ at $t = 1$ is denoted by:

$$S_{1pv} = S(x = 1, t = 1), \tag{35}$$

and is described by the continuous part of the BL solution (a saturation above the front saturation) with velocity:

$$\frac{dx}{dt} = f'(S_{1pv}) \tag{36}$$

This saturation can be found from solving:

$$x = f'(S_1) \cdot 1 = 1, \quad S_1 = (f')^{-1}(1) \tag{37}$$

The average water saturation (and hence recovery of mobile oil) at $t = 1$ is given by:

$$\begin{aligned}\overline{S}(t=1) &= \int_{x=0}^{x=1} S(x,t=1)dx = \int_{S=0}^{S=S_{1pv}} dS + \int_{S=S_{1pv}}^{S=1} x(S)dS \\ &= S_{1pv} + \int_{S=S_{1pv}}^{S=1} f'(S)dS = S_{1pv} + f(1) - f(S_{1pv}) \\ &= S_{1pv} + 1 - f(S_{1pv}) = S_{1pv} + \frac{1}{1+M(S_{1pv})}\end{aligned} \tag{38}$$

It is seen that both S_1 and $M(S_1)$ must be known to uniquely determine recovery. Hence, all single parameter approaches used to scale recovery will only be approximations when the $M(S)$ relation is allowed to vary (e.g. due to variation in viscosity or relative permeability relations).

Appendix B. Convergence

Sensitivity to numerical parameters was tested by reducing grid block dimensions $\Delta x, \Delta z$ (both by a factor 1.5 or 2) and the maximum allowed time step for implicit calculations Δt (from 365 d to 1.5 or 1 d). We note that the timestep in practice was limited by changes in saturation and pressure and thus far less than 365 d. For challenging cases where hysteresis, heterogeneity, gravity and WAG injection were all relevant, the numerical settings had some effect, see Figure 16, and resulted in at most ≈ 5 units difference in recovery after 1.5 PV = 3650 d. Usually the difference was far less.

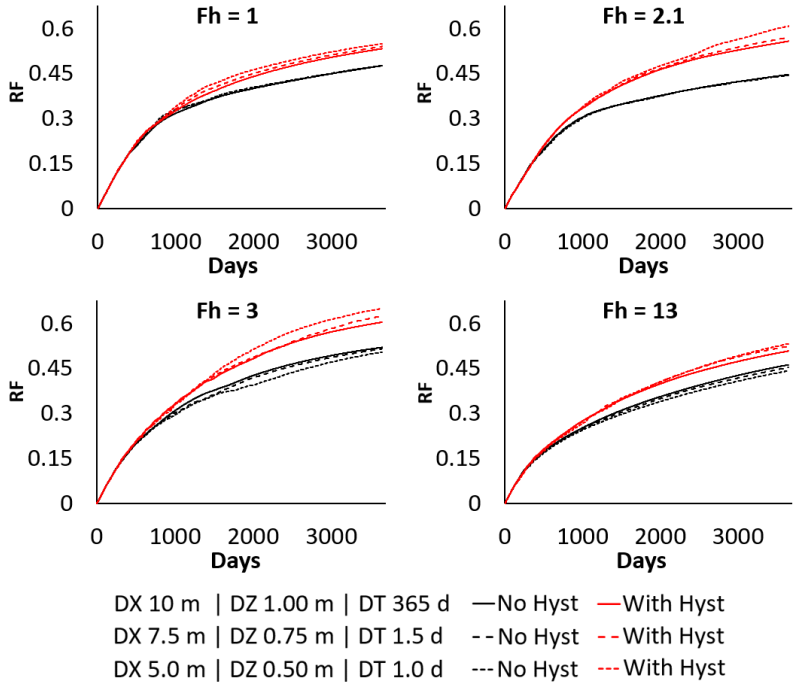

Figure 16. Sensitivity to grid specifications for the base case with WAG injection ($r_w = 0.5$) and gravity ($\Delta\rho = 400$ kg/m^3) effects.